Technical University of Denmark

Final project: Group # 5 - Crocodile

Course:
41525: FEM-Heavy

Author(s):

Laura Stokbro (S123155): s. 1-2 s. 5-6, s. 12-15
Lauge Kongstad (S123896): s. 3-4, s. 9-12

November 27, 2017

Table of Contents

1 Plate theory

1.1

As seen in fig.1, a bending plate can be described by z- displacement (w), and rotations around the y-direction (θ_y) and rotations around x-direction (θ_x). These will also be the degrees of freedom in the FEM-model. From 3.1-9 [Cook2002] we have:

$$u = z\theta_y \quad v = -z\theta_x \quad \epsilon_x = z\theta_{y,x} \quad \epsilon_y = -z\theta_{x,y}$$

$$\gamma_{xy} = z(\theta_{y,y} - \theta_{x,x}) \quad \gamma_{yz} = w_{,y} - \theta_x, \gamma_{yz} = w_{,x} + \theta_y$$

We have implemented the Kirchhoff element and here transverse shear deformation is prohibited. so $w_{,x} = -\theta_y$ and $w_{,y} = \theta_x$. From the equations above we can find the internal energy of the Kirchhoff plate:

Figure 1: Plate

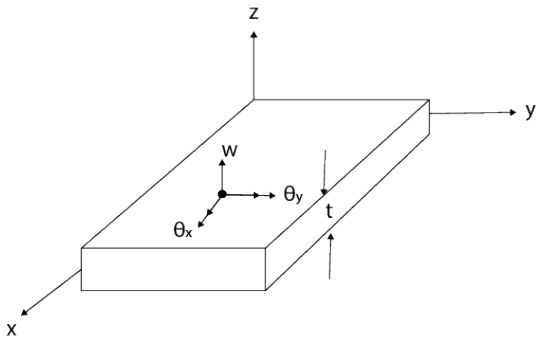

$$\epsilon_x = -zw_{,xx} \qquad \epsilon_y = -zw_{,yy} \qquad \gamma_{xy} = -z(w_{xy} + w_{xy}) \tag{1}$$

we define

$$\kappa = \left\{ \frac{d^2}{dx^2}, \frac{d^2}{dy^2}, 2\frac{d^2}{dxdy} \right\}^T w \tag{2}$$

and therefore we have.

$$U = \int_V \{\delta\epsilon\}^T [C]\{\epsilon\} dV \Rightarrow U = \int_A \{\delta\kappa\}^T [D]\{\kappa\} dA \tag{3}$$

where $[D] = \frac{1}{12}t^3[C]$.

Now we can use the VWP principle to derive the discrete equation of the plate problem.

$$\int_A \{\delta\kappa\}^T [D]\{\kappa\} dA = \int_{S_F} \left\{ 1, \frac{d}{dx}, \frac{d}{dy} \right\}^T \delta w\{F\} dS + \sum_i \delta w\{p_i\} \tag{4}$$

$\sum_i \delta w p_i$ are the point loads and $\int_{S_e} \{1, \frac{d}{dx}, \frac{d}{dy}\} \delta w\{F\} dS$ are the surface loads. From 15.2-2 [Cook2002] we have:

$$w = \{N\}^T\{d\} \quad \rightarrow \quad \{\kappa\} = [B]\{d\} \quad \text{where} \quad [B] = \left\{ \frac{d^2}{dx^2}, \frac{d^2}{dy^2}, 2\frac{d^2}{dxdy} \right\}^T \{N\} \tag{5}$$

By inserting, rearranging and summing over the elements of eq. (4), we can derive the descrete formula used to develop the code in Fortran:

$$\sum_e \int_{A_e} [B]^T [D][B] dA\{D\} = \sum_e \int_{S_e} \{N\} \left\{ 1, \frac{d}{dx}, \frac{d}{dy} \right\} dS\{F\} + \{P\} \tag{6}$$

The element stiffness matrix is $ke = \int_{A_e} \frac{1}{2}[B]^T[D][B]dA$. The matrix $[D]$ is the matrix described in eq. (3), whereas the vector $\{D\}$ is the displacement vector. The surface loads are: $\int_{S_e}\{N\}\left\{1, \frac{d}{dx}, \frac{d}{dy}\right\} d\{F\}$ and $\{P\}$ is the point load vector. We have chosen to work with rectangular Kirchhoff elements. Here the displacement w is described as a twelve term polynomial:

$$w = \{X\}^T\{a\} = \{1, x, y, x^2, xy, y^2, x^3, x^2y, xy^2, y^3, x^3y, xy^3\}\{a\} \tag{7}$$

. $\{a\}$ is the generalized dofs. The displacements can then be described as

$$\{d\} = [A]\{a\} \tag{8}$$

$$\{d\} = \{w_1, w_{,x1}, w_{,y1} ...w_{,y4}\}^T \tag{9}$$

From eq. (7),(8) and (9) $[A]$ can be found. From eq. (5),(7) and (8) the shape function can be found as:

$$\{N\}^T = \{X\}^T[A]^{-1} \tag{10}$$

From eq.(1), (2) and (5) we find the strain:

$$\{\epsilon\} = -z\left\{\frac{d^2}{dx^2}, \frac{d^2}{dy^2}, 2\frac{d^2}{dxdy}\right\}^T w = -z\kappa = -z[B]\{d\} \tag{11}$$

The stress can be computed as for the continuum problem: $[C]\epsilon$

To make the Fortran code able to analyze plates by discretizing them into rectangular Kirchhoff elements, the code had be changed so that it could handle 3 DOFs for every node $(w, w_{,x}, w_{,y})$. Therefore changes in the EDOF calculation, the assembling of the load vector and the element stiffness matrix needed to be made. The components of the element stiffness matrix was found in Maple. First the shape function was found (eq.10). The $[B]$ matrix was found by differentiating the shape function twice with respect to x and y (eq.(5)). Then the term $[B]^T[D][B]$ was integrated over the area of the element(from $x = -a..a$ and $y = -b..b$). Now the components of the element stiffness matrix could be found and inserted into the subroutine *shell41_ke*.

The contribution from the surface loads to the the load vector is calculated in *shell41_ss*. There are three different types of surface loads that can be applied to the Kirchhoff element: surface pressure in the z direction, line moment around the y-direction and line moment around the x-direction. This is also corresponding to the three rows of the $\{F\}$- vector from eq. (6). $\{F\} = \{p_z, M_{xx}, M_{yy}\}$.The contribution from the surface pressure in the z-direction was found by integrating the shape function over the area of the element where the surface load is applied(This was done in Maple) and multiplying it by the pressure.

The contribution from the line moment around the y-direction was found by differentiating shape function with respect to x and integrating it over the height(-b..b) of the element where the line moment is applied(This was done in Maple) and multiplying it by the line moment. The same was done to find the line moment around the around the x-direction but differentiating the shape function with respect to y and integrating over the height of the element(-a..a).

1.2 Limitations of the Kirchhoff elements

There are quite some limitations of the Kirchhoff elements. First of all transverse shear strain is not prohibited in the element. The error due to this simplification will be significant for large deflections as the plate cannot contract or elongate when heavily loaded.

Another limitation is that the Kirchhoff element is 2D but representing 3D-geometry. The thickness of the Kirchhoff element is an attribute and not geometric.

The Kirchhoff element is therefore suitable for thin plates with small deformations only, and not for thicker plates where the transverse shear strains are not neglegible.

A third limitation is the rectangular geometry of the elements which means that if chosen to describe a geometry which is not rectangular, the connection between the elements will not be smooth. This effect will cause problems when evaluating the stress in and the strain in the boundary region between two elements.

1.3 Eigenvalue theory

The mass element matrix was found by same procedure as notes of chapter 9, but using the shape functions described above

$$\int_V \rho[N]^T[N]dV$$

$$\int_{-a}^{a}\int_{-b}^{b}\int_{-t/2}^{t/2} \rho[N]^T[N]dxdydz$$

This was calculated in maple and imported in to the FORTRAN code.

For a simple supported isotropic rectangular plate the (m,n)-eigenvalue is given by *"Introduction to analysis and design of plate panels", Juncher* page 60 as eq. 12

$$\omega_{m,n} = \sqrt{\frac{D}{\rho \cdot t}} \cdot \pi^2 \left(\left(\frac{m}{a}\right)^2 + \left(\frac{n}{b}\right)^2 \right) \tag{12}$$

$$D = \frac{E \cdot t^3}{12 \cdot (1-\nu^2)}$$

Where E is youngs modulus, t is the plate thickness, a and b are sides of the plate, ν is possion ratio, ρ is density.

1.4 Topology optimization

In this project we have used topology optimization to minimize the compliance and thereby the displacements of the plate. The objective function of an arbitrary function of the relative element densities ρ can be written as $f(\{\rho\})$. Now the optimization problem that we wish solve can be formulated as:

$$\min : f(\{\rho\}), \quad \text{s.t.} \quad g(\{\rho\}) = \{v\}^T\{\rho\} - V* < 0, \quad \{0\} < \{\rho_{min}\} \leq \{\rho\} \leq \{1\}$$

In order to implement the topology optimization of plates we have used the theory from the lecture notes from chapter 4 and the code developed in week 4. In addition we have implemented a filtering of the mesh to avoid the checkerboard effect, which is a configuration of elements that has an artificially high stiffness. The checkerboard effect can occur when using Q4 elements if the optimal distribution of material in an area of the structure is $\rho = 0.5$. If the penalty factor is set higher than 1 the optimal structure in this area becomes a checkerboard structure which has artificially high stiffness, since the stiffness matrix will contain artificially high values since the element stiffness matrix is multiplied by $\rho_e^{penalty}$(Topopology Optimization" by M. P. Bendsøe and O. Sigmund). With inspiration from the article [Sigmund2001] we have developed filtering of the elements. The filtering takes a weighted average of the *derivatives of the compliances* (DoCs) of elements within a certain radius. For every element the filter program finds the surrounding elements(within a given radius), computes the weighted average of the DoCs and saves it into a vector that will in the end be the new DoCs of the elements. With the new DoCs the program finds the global minima of the compliances and thereby calculates the relative densities.

The way that the filter algorithm finds the surrounding elements within the given radius, is to loop over every element to check if it is within the radius of the element which DoC needs to be updated. It has to do this for every element which can be a quite costly procedure. If it is known exactly how the elements are numbered in the mesh, there are less costly alternatives to find the elements within the radius. We have chosen the above described procedure, because it can be used for all types of meshes (structured and unstructured) and therefore is robust.

In addition we have designed the code so that it possible to find the optimal structure when different load cases are applied. This requires the code to take the weighted average of the DoCs for every load case and find the global minima for using the weighted DoC. Therefore it is possible to write an extra input to the input file representing which load case each load is a part of. In *fea.f90* we loop over the loadcases when finding the DoCs and after this loop the weighted average of the DoCs of the different loadcases is found.

2 Analytical and Numerical solutions compared

2.1 Point load

To test the FEM code we have analysed a 10x10 simple supported square plate. Where a point load of the value 0.1 is applied in (x,y)=(7.5,7.5). The thickness of the plate was set to 1, the Young's modulus to 1 and the Poisson's ratio to 0.3. The analytical displacement solution is found by the Navier method. [Pedersen1998]

The displacement in (7.5,7.5) converges from above(see fig. 2a). The error is proportional to the squared length og the element h^2 as the displacement decreases in a straight line in fig. 2a. The maximum displacement does not converge in a straight line, because depending on the mesh the FEM model finds the maximum displacements in different places. This can be seen in table 1.

The maximum Von Mises stress (VMs) does not converge (fig. 2b). This is because the stress where the point load is applied is infinitely big. The smaller the elements the bigger the stress because the force is distributed over a smaller area.

The Von Mises Stress in (x,y)=(5,5) does converge quite fast. (fig.2c)

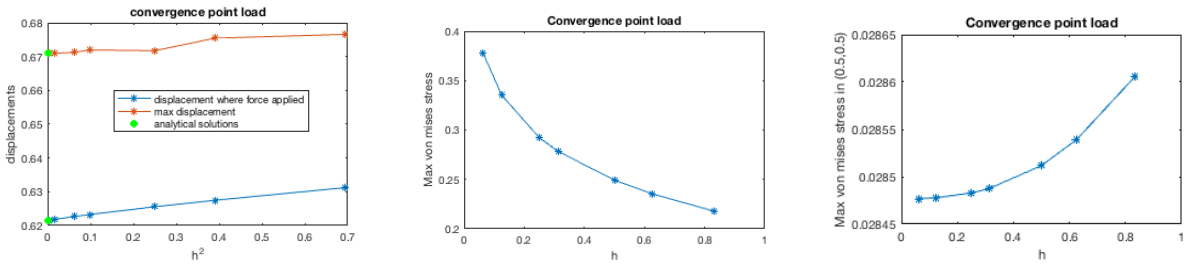

(a) Displacement convergence (b) Max Von Mises stress (c) VMs in (x,y)=(5,5)

Figure 2

h	Analytical solution	0.8333	0.6250	0.5000	0.3125	0.2500	0.1250
(x,y) max displacement	(6.88,6,88)	(6.67,6.67)	(6.88,6.88)	(7.0,7.0)	(6.88,6.88)	(6.75,6.75)	(6.88,6.88)

Table 1

2.2 Surface load

The same 10x10 simply supported plate as used to test the point load has been used to test the surface load versus the Navier analyticaæ solution[Pedersen1998] [Timoshenko and Woinowsky-Krieger1959] for surface loads. Everywhere on the simply supported plate a pressure of 0.1 has been applied. In fig. 3a it is seen that the displacement converges from above towards the analytical Navier solution. The error is proportional to the length og the element h^2 as the displacement decreases in a straight line in fig. 3a.

In fig. 3b the convergence of the maximum VMs is shown. When the VMs is evaluated in the middle of the element it converges from below(Blue line and stars). When evaluted in the corner of the element it converges from above (red line and stars).

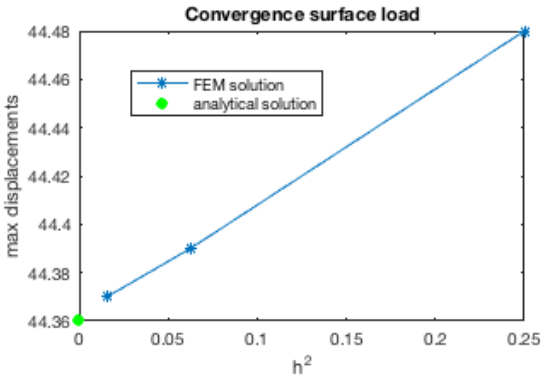

(a) Max. Von Mises Stress Convergence

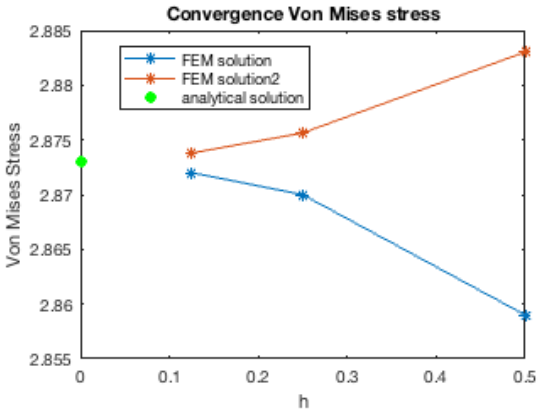

(b) Max. displacement convergence

Figure 3

2.3 Moment load

The same 10x10 simply supported plate as used to test the point load and the surface load has been used to test the line moment versus the Levy analytical solution[Lévy1899][Pedersen1998]. A line moment ($M_{yy} = 0.1$) around the x-direction has been applied to the edge $y = 0$ and a line moment $M_{yy} = -0.1$ has been applied to $y = b$. Hence the load case is a symmetrical uniform distributed moment load. In fig. 4a it is seen that the displacement converges from above towards the analytical Levy solution. The error is proportional to the length of the element h^2 as the displacement decreases in a straight line in fig. 4a.

In fig. 4b the convergence of the VMs is shown. We have chosen to make the convergence check of VMs by evaluating the VMs in the middle of edge where the line moment is applied ($y = 0, x = 5$). The maximum VMs will not converge since the maximum VMs is found in the corners of the plate and here the VMs will approach infinity if it is a perfectly sharp corner.

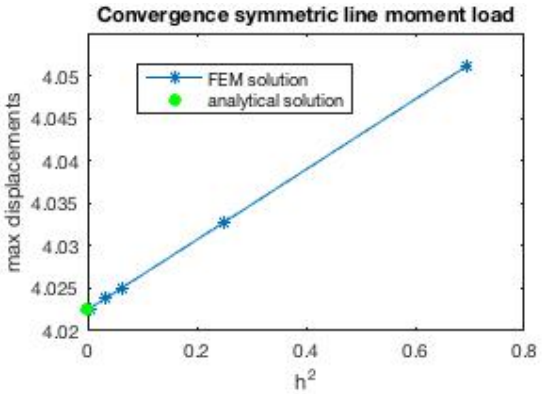

(a) Max. displacement convergence

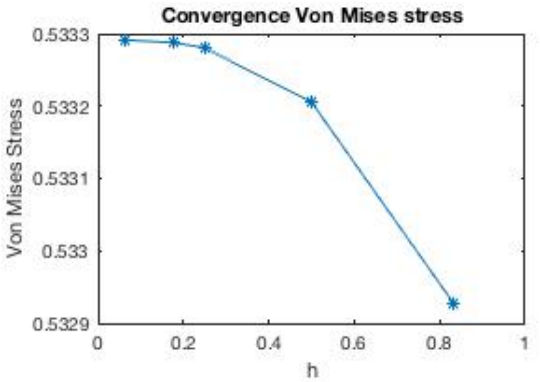

(b) Von mises stress convergence

Figure 4

2.4 Eigenvalues and -modes

Test case: square plate with $a = 1$, $b = 1$, $t = 1$, $E = 1$, $\rho = 1000$, $\nu = 0.3$ was used. The first 10 eigenvalues was found using FEM and eq. 12. Results are shown in fig. 5 and 6.

In fig. 5a the results are shown with the analytical values at 0 on the x-axis. As expected the the eigenvalues converges towards analytical solutions. In fig. 5b the errors of the finest mesh (a 30x30 mesh with $h = 0.033$) are shown, which shows a trend of larger errors for higher eigenvalues, with one exception of eigenvalue 4.

Some of the eigenvalues appear to have the same values (2 &, 5 & 6 and 7 & 8). This could be explained by the corresponding eigenmodes, which look the same only mirrored, see fig. 6b & 6c and fig. 6g & 6h. However the 5th and 6th eigenmodes fig. 6e & 6f does not follow this.

It is noticeable that for the first eigenvalue in fig. 5a the approximation with the largest element size used (a 3x3 mesh with $h = 0.33$) is actually pretty accurate. However for the highest eigenvalues the difference is large and the largest eigenvalues "melt together". This makes sense as the eigenmode is complex and the coarse mesh might not have enough dof to describe the eigenmodes. The eigenmodes have been compared with results of a plate in vacuum [Zhangming Wu2009] and showed good resemblance.

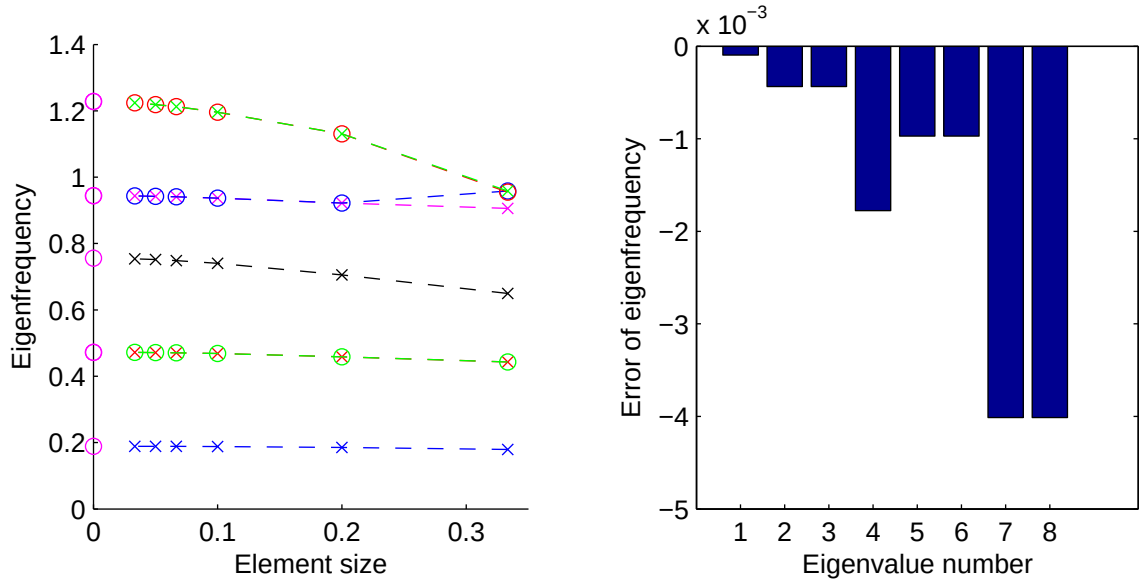

(a) Convergence of eigenvalues

(b) Error of eigenvalues for $h = 0.033$

Figure 5: Comparing numerical and analytical solutions of eigenvalues

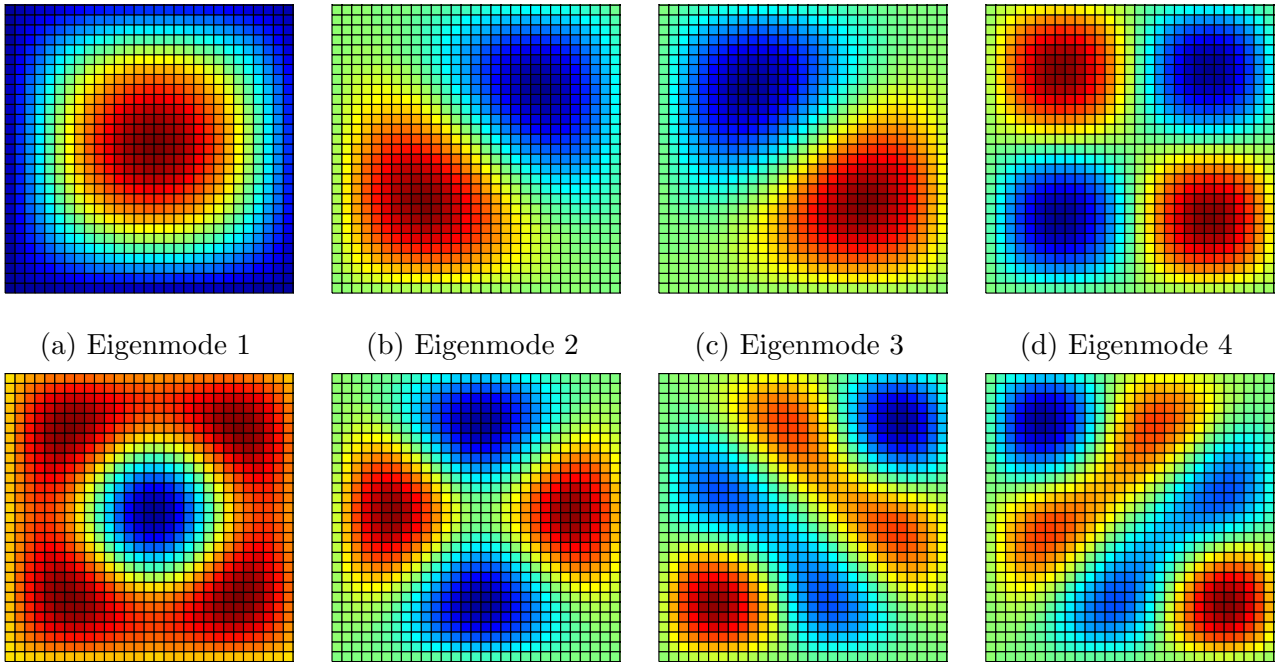

(a) Eigenmode 1 (b) Eigenmode 2 (c) Eigenmode 3 (d) Eigenmode 4

(e) Eigenmode 5 (f) Eigenmode 6 (g) Eigenmode 7 (h) Eigenmode 8

Figure 6: First 6 eigenmodes found with finest mesh $h = 0.033$

Advanced example: Guitar

In order to design well functioning musical instruments knowledge of the structure is important. It was attempted to predict the eigenmodes and -frequencies of a guitar, when only modelling the front panel, see results in fig. 7. The results was compared with an investigation of a guitar using COMSOL [Marttila2011] which showed decent results for the two first eigenmodes, but the rest differed quite a bit. An explanation of this could be the crude geometrical simplification (shape, size), the 2D simplification which also lead to the clamped boundary conditions and the fact that the physics of the fluid interaction inside the guitar is not modelled either. Furthermore the material properties could also have an impact on this. A conclusion must be that the problem is too complicated for the plate model used in this assignment.

No eigenfrequencies was readily available and therefore difficult to evaluate, which is why they aren't showed here.

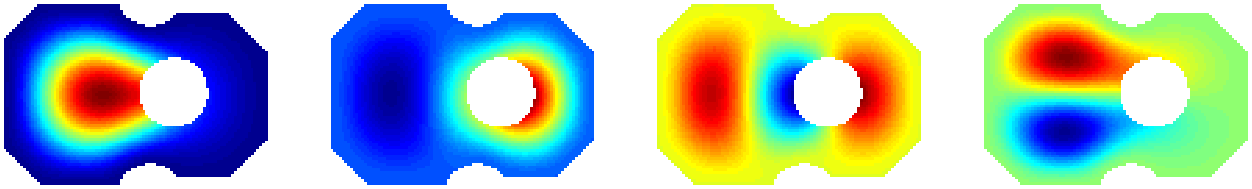

(a) Eigenmode 1 (b) Eigenmode 2 (c) Eigenmode 3 (d) Eigenmode 4

Figure 7: First 4 eigenmodes of the guitar

3 Topology Optimization

3.1 Test cases

Different test cases where carried out using the implemented topology optimization. The test cases presented in the following were chosen either because they where simple and it was possible to predict an optimal structure, or because they showed interesting results worth discussing.

Test case A: A design domain of 100 m x 100 m x 1 m with 2500 square elements was created. One side was fully clamped and a point load was introduced far from the clamped end. The optimization was performed with $p = 3.0$, $\eta = 0.5$ and $V^* = 0.3$. Material properties was $E = 1000$ and $\nu = 0$, results are seen in fig. 8. The compliance converges with number of iterations as expected, and in the rest of the report this plot will not be shown unless odd behaviour is encountered. The energy density is relatively constant, which is expected as this is what the optimization attempts to achieve. The optimized structure is wider in the end of support than at the load. This make sense as the moment varies with maximum value at the support and 0 in the free end.

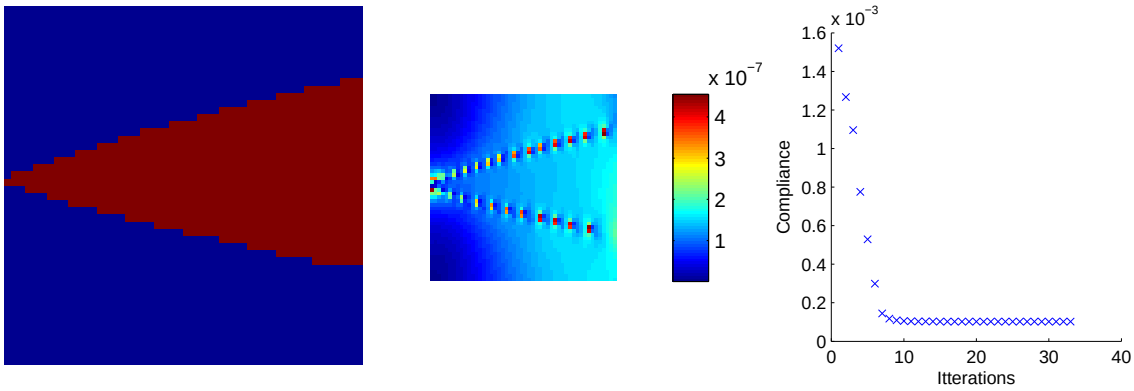

(a) Relative dens. $\nu = 0$ (b) Strain energy dens. $\nu = 0$ (c) Compliance $\nu = 0$

Figure 8: Load case A

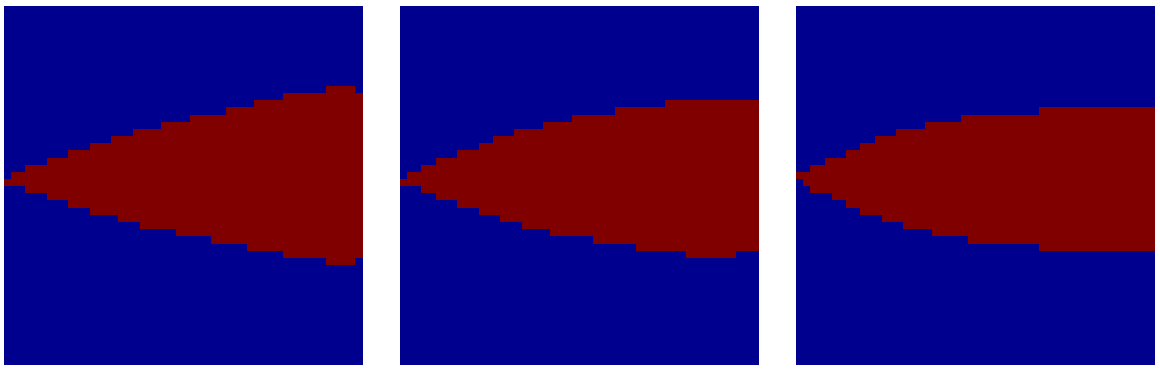

(a) $\nu = 0.1$ (b) $\nu = 0.3$ (c) $\nu = 0.6$

Figure 9: Different ν

The effect of poissons ratio is investigated both with and without topology optimization, seen in fig. 10. "No topology" meaning that it is a full plate where only Poissons ratio is varied. The displacement decreases with increasing Poissons ration as expected: Poissons couples the moment of X with the moment of Y as stated in Cook page 533 eq. (15.1-4b). This will make the plate curl at the edges which could increase the stiffness of the structure. For "Topology" the displacement actually increases for small Poissons ratios, which is difficult to explain. It could be because the optimization algorithm had not found the best minimum. The structures are shown in fig. 9, where it is seen that the structures tend to put more material towards the load and less at the support. This makes sense as the moment is largest near the support and therefor the stiffening effect caused by Possion ratio is also the highest. Therefore it can better afford to put more material towards the load.

Test case B: A design domain of 10 m x 10 m x 0.1 m with 1024 square elements was created. All sides were fully clamped and a point load of 0.1 was introduced in the center dof. The opimization was perfomed with $p = 3.0$, $\eta = 0.5$ and $V^* = 0.3$. Results are seen in fig. 11c. The structure consists of a square and 4 "arms" which look similar to that of test case A: widest

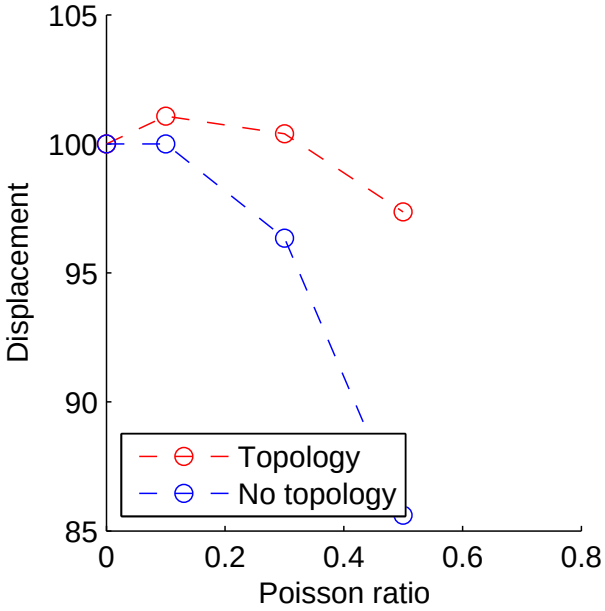

Figure 10: Displacement v. ν

near the support and thinnest/lowest density in the middle. The arms are connected to the sides of the design domain, and not in the corners, which makes sens as the corners are further away and therefore more expensive in terms of volume to use as fix points. The structure can be explained by moment curve seen in fig. 13a, where the moment between the load point and the support is zero. At the corresponding point at the structure the density is very low.

The effect of different penalty factors was also examined shown in fig. 11 where the number of elements with intermediate relative densities evident. On fig.12 it is shown that the penalty factor has a large impact on computation time.

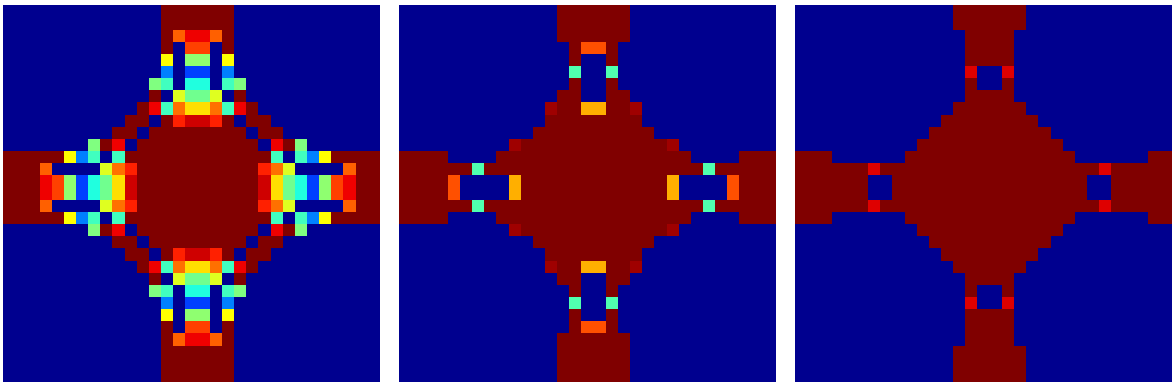

(a) Relative density p = 1.5 (b) Relative density p = 2.0 (c) Relative density p = 3.0

Figure 11: Test case B

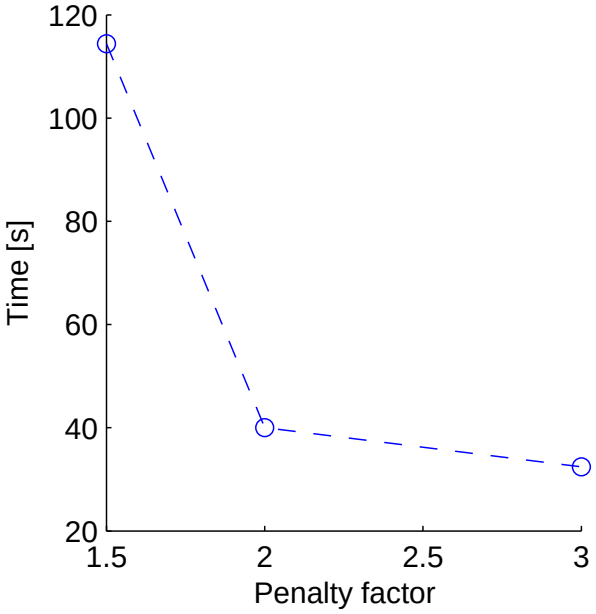

Figure 12: Time v. penalty factor

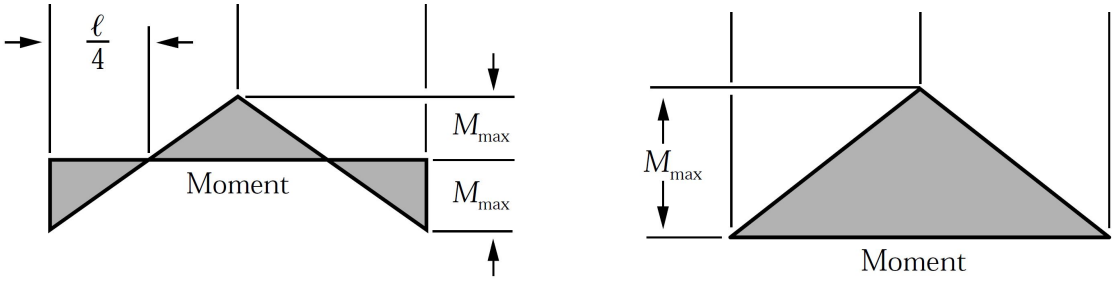

(a) Clamped in both ends

(b) Simple supported in both ends

Figure 13: Moment curves: Load at mid point, different supports

Test case C: A design domain of 10 m x 10 m x 1 m with 1024 square elements was created. All sides were simply supported and a point load was introduced in the center node. The optimization was performed with $p = 2.0$, $\eta = 0.5$ and $V^* = 0.4$. Results are seen in fig. 14a. The structure consists of a square with large checkerboard effect and arms connected to the supports.

The arms in the diagonal is attached in the corners, which makes sense physically as this effectively is a fully clamped support as the ones discussed above. The arms connected to the sides of the domain looks more like hinges and have low density / few elements at the boundary. This can be explained by the moment curve seen in fig. 13b, where the moment is zero at the supports and is maximum at the load.

Filter: The checkerboard phenomenon is observed where the arms attach to the square, and it is therefore relevant to employ the filter and investigate the effect. The effect of the filter is shown in fig. 14a - 14c. Fig. 14d shows that the max displacement / compliance increases as

a filter radius increases, which makes sense as the optimization algorithm is forced away from the minimum. It should be noted that this minimum found without the filter would never work in real life. It is obvious that the checkerboard disappears which shows the filter is working as intended but it is also clear that using the filter changes the design quite a lot. This shows that employing the filter has a big impact on the optimization.

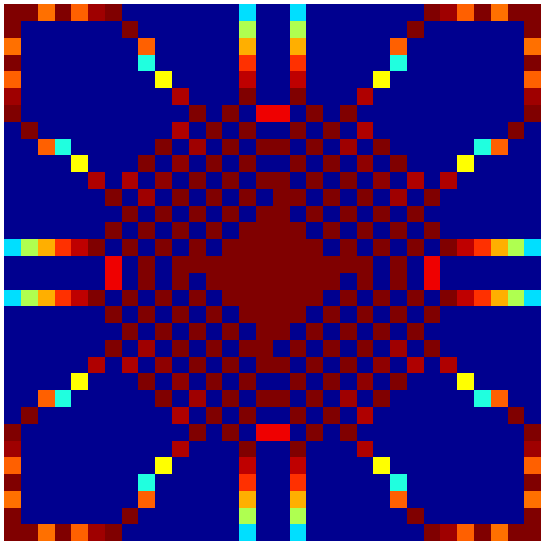

(a) $r_{min} = 0$

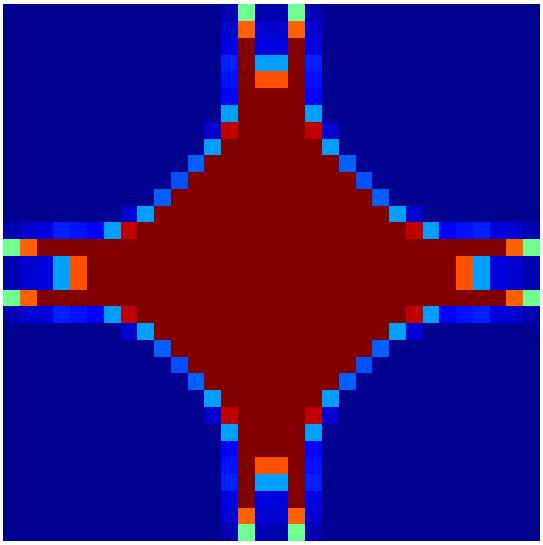

(b) $r_{min} = 1.1$

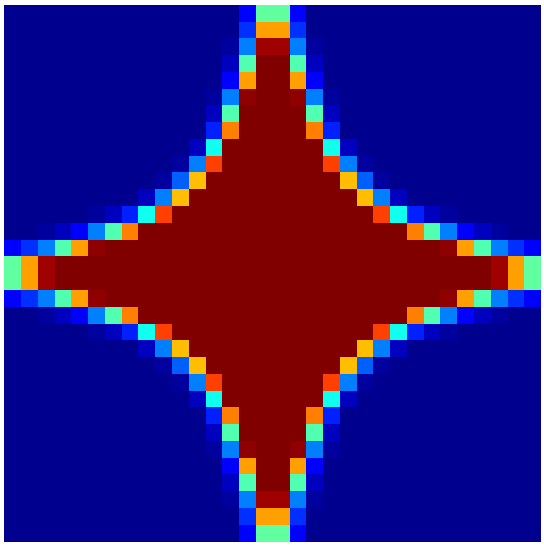

(c) $r_{min} = 2.1$

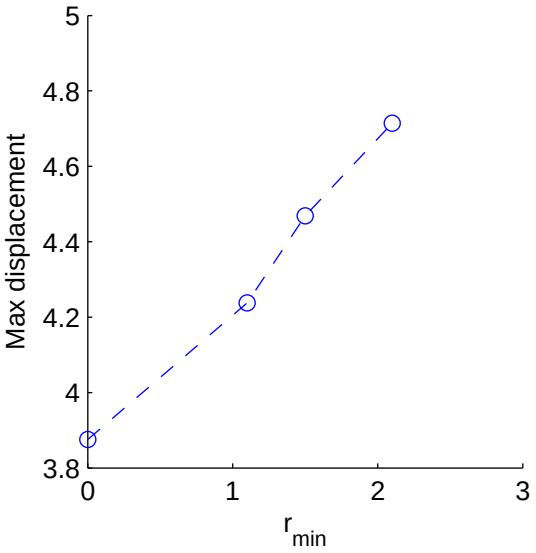

(d) Stiffness

Figure 14: Filter effect

3.2 The Drone example

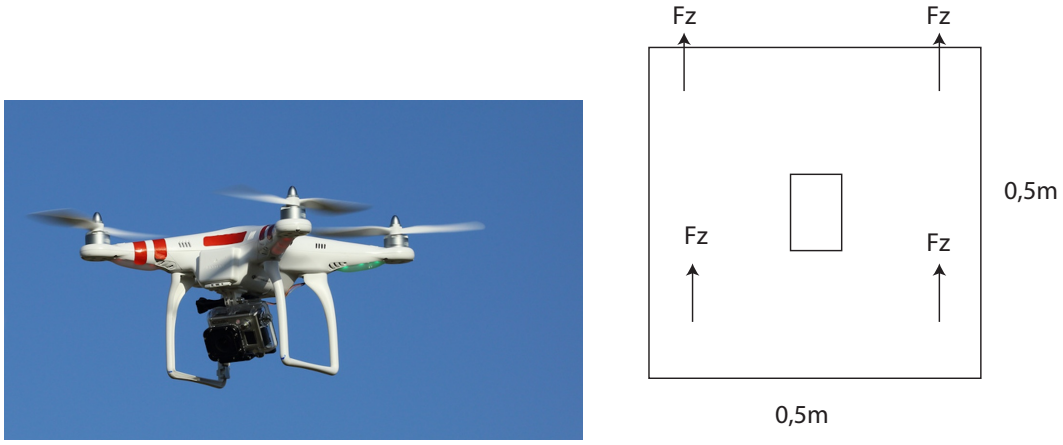

(a) Drone with camera (b) Design domain

Figure 15: Drone example

This example investigates the optimal design of a plate used as the base plate of a drone when a minimum deflection is wanted. The plate has a thickness of 5mm and four rotors are mounted which are represented as forces fig. 15b. The material chosen is aluminium with $E = 69$ GPa, $\nu = 0.3$ The design domain available is 50cm x 50cm. It is assumed that there is existing components such as electronics, batteries etc. (which cannot obtain loads) protected in a very rigid casing in the middle of the drone(fig. 15b. This is simplified as an area of removed elements which have clamped supports to the rest of the design domain.

Two different load cases are investigated:
Load case **Rise** where all 4 rotors are engaged. The mass of the drone is assumed 1kg and an upward acceleration of 6 $\frac{m}{s^2}$ is wanted which leads to $Fz_{total} = 16$h N and $F_{rotor} = 4$ N on each rotor, by newtons 2nd law.
Load case **Turn** resembles a sharp turn of the drone where only 2 of the rotors are engaged with $F_{rotor} = 4$ N.

The optimizations are run with $p = 3.0$, $\eta = 0.5$, and a max volume fraction of 0.1 pr. load. This means that we optimize with $V^* = 0.4$ for Rise and $V^* = 0.2$ for Turn. The load cases are investigated separately fig. 16a & 16b. It is clear when investigating these results that if one uses the structure optimized by Rise this would perform poorly at Turn, and vice versa.

The case of multiple loads are shown in fig. 16c. This structure is not optimized towards one of the load cases so it would perform averagely, but not excel in either load case.

In figure fig. 16d-16f an investigation of different volume fractions are carried out for the multiple load cases.

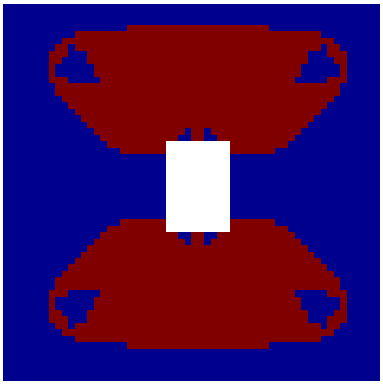

(a) Rise load $V^* = 0.40$

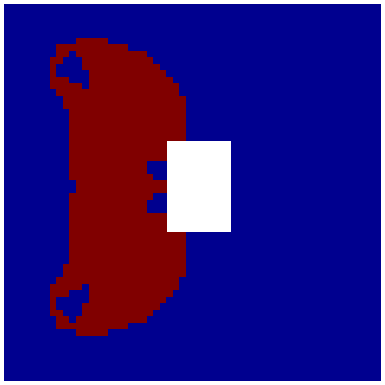

(b) Turn load $V^* = 0.20$

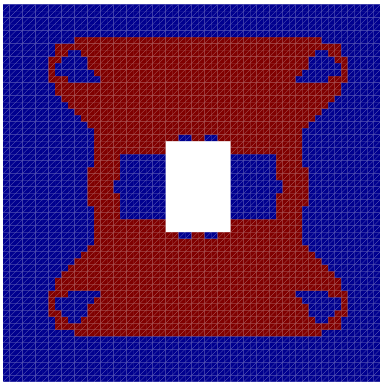

(c) Multiple load $V^* = 0.40$

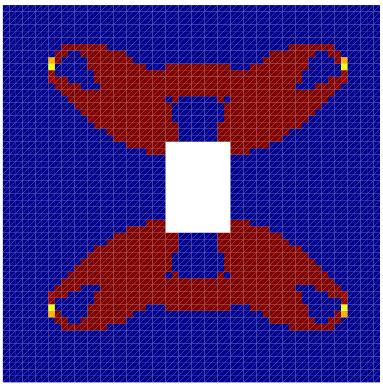

(d) Multiple load $V^* = 0.25$

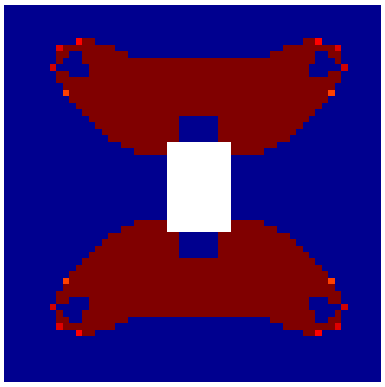

(e) Multiple load $V^* = 0.30$

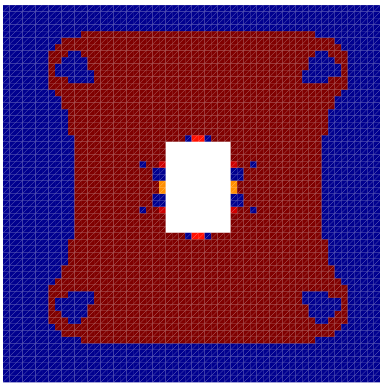

(f) Multiple load $V^* = 0.50$

References

[Cook2002] Robert D. Cook. *Concepts and Applications of Finite Element Analysis*. Wisley, 2002.

[Lévy1899] M. Lévy. *Comptes rendues*. 1899.

[Marttila2011] Pasi Marttila. Virtual guitar. 2011.

[Pedersen1998] Pauli Pedersen. *Elasticity - anisotropy - laminates*. DTU, 1998.

[Sigmund2001] Ole Sigmund. 99 line topology optimization code written in matlab. *Review of Scientific Instruments*, 2001.

[Timoshenko and Woinowsky-Krieger1959] S. Timoshenko and S. Woinowsky-Krieger. *Theory of plates and shells*. McGraw-Hill New York, 1959.

[Zhangming Wu2009] Peter N Brett Jinwu Xu Zhangming Wu, Xianghong Ma. Vibration analysis of submerged rectangular microplates with distributed mass loading. 2009.